Lattice Boltzmann model for numerical relativity

E. Ilseven[*] and M. Mendoza[†]

ETH Zürich, Computational Physics for Engineering Materials, Institute for Building Materials, Wolfgang-Pauli-Strasse 27, HIT, CH-8093 Zürich, Switzerland

In the Z4 formulation, Einstein equations are written as a set of flux conservative first-order hyperbolic equations that resemble fluid dynamics equations. Based on this formulation, we construct a lattice Boltzmann model for numerical relativity and validate it with well-established tests, also known as "apples with apples." Furthermore, we find that by increasing the relaxation time, we gain stability at the cost of losing accuracy, and by decreasing the lattice spacings while keeping a constant numerical diffusivity, the accuracy and stability of our simulations improve. Finally, in order to show the potential of our approach, a linear scaling law for parallelization with respect to number of CPU cores is demonstrated. Our model represents the first step in using lattice kinetic theory to solve gravitational problems.

I. INTRODUCTION

General relativity was introduced by Albert Einstein in 1915 and became the first geometric theory of gravitation. It includes ten nonlinear second-order differential equations and due to their complexity, few analytical solutions are known. Therefore, numerical methods have played an important role in recent decades. Solving Einstein equations numerically is often called "numerical relativity."

With the 2005 breakthroughs in numerical relativity [1–3], it is now possible to simulate compact binary coalescenses. This includes binary black hole merger, binary neutron star mergers, and neutron star-black hole mergers. Most of the popular methods for solving these equations are based in finite differencing [4] or pseudospectral techniques [5]. While there is a great effort to solve more complicated phenomena, there is also much work done in solving technical problems encountered during the numerical simulations. Such problems, especially in highly curved spacetimes, are tackled by mathematical corrections, such as conformal and isometric mappings [6], or by numerical methods, such as exponentially growing lattice spacings or adaptive mesh refinements [7]. Complicated geometries and singularities leading to highly curved spacetimes are also handled by excision and moving puncture methods. Additionally, improving the parallelization efficiency of current methods still represents a challenge in numerical relativity.

There are several mathematical formulations of Einstein equations (see Ref. [8] for more details) that are useful for numerical relativity simulations. These include the generalized harmonic approach [1,5,9] and variations of the Arnowit-Deser-Misner (ADM) 3+1 decomposition. The latter includes the BSSNOK system [10–12] and the Z4 systems [13]. In this work, we use the Z4 formulation of Einstein equations, since it consists in first-order hyperbolic conservation equations for the geometric variables [14,15], resembling fluid dynamics equations, and therefore, making suitable the use of fluid dynamics solvers. This formalism is connected to the BSSNOK and Bona Masso formalisms by an explicit symmetry breaking [16].

In this paper, we propose for the first time a lattice Boltzmann model to solve Einstein equations. Usually, the lattice Boltzmann method allows us to solve the Navier-Stokes equations (or any conservation law) to an accuracy that depends on the Knudsen number (roughly defined as the ratio of lattice spacing to system size) [17]. This method has been successfully used to study many physical systems using a fraction of computational time of other numerical methods [18–23]. Here, we extend the wide applicability of the lattice Boltzmann method to gravitation. Furthermore, we investigate the performance of the model with the following well-established apples with apples tests reported in Ref. [24,25].

A. Expansion of a flat universe

We simulate an expanding flat universe and compare the results with the expected analytical solution. This example uses an ideal fluid energy-momentum tensor and shows that it is coupled correctly to the rest of the model variables.

B. Robust stability test

In this test all dynamical fields are initiated as flat space with random noise to test the capability of the model to handle errors.

C. Gauge wave

We test the ability of the scheme to propagate a gauge wave. The gauge wave is achieved through a nonlinear coordinate transformation, which does not change the physics at hand.

D. Linear wave

We validate the model propagating the amplitude and phase of a gravitational wave, i.e., a spatial transverse wave propagating in x direction and time.

E. Shifted gauge wave

While in the gauge wave test only the diagonal elements of the metric were evolved, in this test a nondiagonal temporal element is also evolved.

---

[*]eilseven@student.ethz.ch

[†]mmendoza@ethz.ch

F. Polarized Gowdy wave

A standing wave in an expanding universe is tested. It is a complicated test that involves a stronger curvature than in previous tests and a T^3 topology.

G. Numerical diffusivity

We investigate the role of numerical diffusivity in our simulation errors. While it is normally added artificially in other methods through an elliptic equation [1,6], it is present in the lattice Boltzmann model naturally.

H. Parallelization

We show that our lattice Boltzmann model is well suited for parallel computing. The improvement in the computation duration for a gauge-wave simulation is also shown.

Compared to common methods in numerical relativity, such as finite differences, lattice Boltzmann methods have extra properties that may lead to improvements or short comings, which still need to be tested. Some of them can be listed as follow: The numerical diffusivity in numerical relativity is an extra term introduced in finite difference methods (see Refs. [1,6]) to suppress high-frequency instabilities, while it is naturally present in the lattice Boltzmann method. Our model uses a lattice that offers more isotropy than center-finite differences for calculating spatial derivatives, thus, providing more accurate results when it comes to solving hyperbolic equations; and finally, for simple cases, the lattice Boltzmann method sets time steps equal to the lattice spacing, i.e., space and time scale linearly. Therefore, the present work is just the beginning of a new way of solving the Einstein equation and opens up the door for further research in numerical relativity.

This paper first gives an introduction to numerical relativity and the theory of the specific formulation of the Einstein equations that we have chosen. The lattice Boltzmann method is introduced in the next section. Afterwards, the validation tests are described, and their results using our numerical method are analyzed. In the last section, we summarize our work and discuss possible outlooks.

II. THEORY

Einstein equations are ten coupled second-order nonlinear differential equations that, in their most compact form, are given by

$$R_{\alpha\beta} - \tfrac{1}{2}g_{\alpha\beta}R = T_{\alpha\beta}, \quad (1)$$

where $T_{\alpha\beta}$ is the energy-momentum tensor, $g_{\alpha\beta}$ the four metric and $R_{\alpha\beta}$ the Ricci tensor defined as

$$R_{\alpha\beta} = \partial_\rho \Gamma^\rho_{\alpha\beta} - \partial_\beta \Gamma^\rho_{\alpha\rho} + \Gamma^\rho_{\lambda\rho}\Gamma^\lambda_{\alpha\beta} - \Gamma^\rho_{\lambda\beta}\Gamma^\lambda_{\alpha\rho}, \quad (2)$$

with $\Gamma^\rho_{\alpha\beta}$ the Christoffel symbols,

$$\Gamma^\rho_{\alpha\beta} = \tfrac{1}{2}g^{\rho\lambda}(\partial_\alpha g_{\beta\lambda} + \partial_\beta g_{\alpha\lambda} - \partial_\lambda g_{\alpha\beta}). \quad (3)$$

We use Einstein summation convention throughout the paper and the Greek letters indicate summation over four dimensions, while the Latin letters indicate summation over the three spatial components. Einstein equations, Eq. (1), in their expanded

forms possess very complex shapes and several formalisms are used to ease their solutions.

A. 3+1 Arnowit Deser Misner formalism

The ADM formalism of Einstein equations was first introduced through Hamiltonian framework of general relativity [26,27]. Here, we obtain the ADM formalism with a slightly different construction, as described below. The $3 + 1$ decomposition of Einstein equations lets us find a solution for the four-metric in different hyperspaces, and is given as follows:

$$ds^2 = \alpha dt^2 - \gamma_{ij}(dx^i + \beta^i dt)(dx^j + \beta^j dt), \quad (4)$$

where α and β_i are describing the evolution of hyperspaces in the four-dimensional space, and the hyperspaces (also called slices) are associated with a certain three-metric γ_{ij}. The construction of these geometric objects is given by the following scheme: we construct three-dimensional spaces with the three-metric γ_{ij} and find the normal vector to these spaces, which in contravariant and covariant forms are equal to $(1/\alpha, \beta^i/\alpha)$ and $(\alpha, 0, 0, 0)$, respectively. At every time step we need a variable that describes the evolution of γ_{ij}, which is given by the extrinsic curvature K_{ij}, which is the projection of the curvature to the normal vector onto the three spaces. Due to the symmetry of γ_{ij} (thus K_{ij}) we arrive to six differential equations describing the evolution of the system. Note that other four degrees of freedom are still left, as we are dealing with ten differential equations. These degrees of freedom are covered by the constraint equations, which are energy and momentum conservation. Finally, the ADM equations and constraints are given by the following equations:

$$(\partial_t - L_\beta)\gamma_{ij} = -2\alpha K_{ij}, \quad (5)$$

$$(\partial_t - L_\beta)K_{ij}$$
$$= -\alpha_{i;j} + \alpha\left[R^{(3)}_{ij} - 2K_{im}K^m_j + \text{tr}(K)K_{ij} - R^{(4)}_{ij}\right], \quad (6)$$

$$R^{(3)} - \text{tr}(K^2) + \text{tr}(K)^2 - 2\alpha^2 G^{00} = 0, \quad (7)$$

$$K^j_{i;j} - \partial_i[\text{tr}(K)] - \alpha G^0_i = 0, \quad (8)$$

where L_β corresponds to the Lie derivative along the vector β, $G_{\alpha\beta}$ the energy momentum tensor, and $R^{(4)}_{ij}$ is the projection of the four Ricci tensor on the three-dimensional space. These equations correspond to one representation of the Einstein equations. As we will see later, there can be other formulations. Indeed, all *physical* solutions of the equations match, even if the formulations may not have the same *mathematical* structure. The physical solutions are known to be the solutions belonging to the "constrained space." However, the mathematical differences may increase or decrease the stability of numerical schemes. These two equations can be evolved in two different ways. The first one is letting the system evolve freely and monitor the constraints ("free evolution"), and the second one is solving the constraint equations for each time step for some of the variables and make sure that they are fulfilled ("constrained evolution"). It must be pointed out that the $3 + 1$ decomposition does not lead to an evolution equation for the slicing α and the shift β_i. So we have four additional

degrees of freedom, which we can exploit to improve stability in different systems. Thus, we can formulate

$$(\partial_t - L_\beta)\alpha = -\alpha^2 Q, \tag{9}$$

$$(\partial_t - L_\beta)\beta_i = -\alpha Q_i, \tag{10}$$

where Q and Q_i are gauge functions.

1. Z4 formulation

While there are many ways to solve Einstein equations numerically, the following methods are the most popular ones: BSSNOK (Baumgarte, Shapiro, Shibata, Nakamura, Oohara, Kojima), generalized harmonics, and conformal Z4 formalisms [26]. While ADM tries to solve the equations directly, BSSNOK makes use of conformal mappings and increases the stability of the evolution as conformal variables are evolved. Both formalisms are solved mainly by finite-difference methods. In this work, we will use a third method known as Z4 formalism, which is an extension of the Bona-Masso formalism [13–16,28,29]. It consists in a set of first-order flux conservative hyperbolic equations that are equivalent to Einstein equations. We have seen that Einstein equations, within the ADM formalism, are first order in time derivatives but second order in space derivatives. The Bona-Masso formalism introduces the following space derivatives to obtain first-order differential equations,

$$A_k = \partial_k \ln(\alpha), \quad B_k^i = \partial_k \beta^i, \quad D_{kij} = \partial_k \gamma_{ij}/2, \tag{11}$$

and the Z4 formulation introduces the following dynamical variable $Z_\alpha = (\theta, Z_i)$ to the Einstein equations,

$$R_{\alpha\beta} + \nabla_\alpha Z_\beta + \nabla_\beta Z_\alpha - \tfrac{1}{2} g_{\alpha\beta} R = T_{\alpha\beta}. \tag{12}$$

Note that while in the ADM formalism, energy and momentum conservation equations are solved separately, the evolution equation for Z_α allows us to implement those conservation constraints by ensuring $Z_\alpha = 0$.

B. Z4 evolution equations

Considering the Einstein evolution system, the Z4 equations are given by the following equations:

1. Slicing

$$\partial_t \alpha = \alpha(\beta^r A_r - \alpha Q). \tag{13}$$

2. Shift

$$\partial_t \beta^i = (\beta^r B_r^i - \alpha Q^i). \tag{14}$$

3. Three metric

$$\partial_t \gamma_{ij} = 2\beta^r D_{rij} - 2\alpha(K_{ij} - s_{ij}), \tag{15}$$

$$s_{ij} = \frac{B_{ij} + B_{ji}}{2\alpha}. \tag{16}$$

4. Extrinsic curvature

$$\partial_t K_{ij} + \partial_r\big(-\beta^r K_{ij} + \alpha\lambda_{ij}^r\big) = \alpha S_{ij}, \tag{17}$$

$$\lambda_{ij}^k = D_{ij}^k + \tfrac{1}{2}\delta_i^k\big(A_j + 2V_j - D_{jr}^{\ r}\big) + \tfrac{1}{2}\delta_j^k\big(A_i + 2V_i - D_{ir}^{\ r}\big), \tag{18}$$

$$\begin{aligned}
S_{ij} = {}& -2K_i^k K_{kj} + \mathrm{tr}K\, K_{ij} - 2\theta K_{ij} \\
& + \frac{2}{\alpha}\big[K_{ir}B_j^{\ r} + K_{jr}B_i^{\ r} - K_{ij}\mathrm{tr}(B)\big] + 2D_{ik}^{\ r}D_{rj}^k \\
& + 2D_{jk}^{\ r}D_{ri}^k - \Gamma_{ri}^k\Gamma_{kj}^r - 2D_{rk}^{\ r}\big(D_{ij}^{\ k} + D_{ji}^{\ k}\big) + A_k D_{ij}^k \\
& - \big(A_j D_{ri}^{\ r} + A_i D_{rj}^{\ r}\big) + \tfrac{1}{2}\big(A_j D_{ir}^{\ r} + A_i D_{jr}^{\ r}\big) \\
& + \big(D_{kr}^{\ r} + A_k - 2Z_k\big)\Gamma_{ij}^k - (A_i Z_j + A_j Z_i) - 8\pi(G_{ij} \\
& - \frac{\gamma_{ij}}{2}[\mathrm{tr}(G) - \alpha^2 G_{00})].
\end{aligned} \tag{19}$$

5. Extensions to the model

$$\begin{aligned}
\partial_t Z_k + \partial_r\big(-\beta^r Z_k &+ \alpha\{\delta_k^r[\mathrm{tr}(K) - \theta] - K_k^r\}\big) \\
= \Omega_k = {}& \alpha\{-8\pi\alpha G_k^0 - A_r\big[K_k^r - \mathrm{tr}(K)\delta_k^r + 2\theta\big] \\
& - K_r^j\Gamma_{jk}^r + K_k^r\big(D_{rj}^{\ j} - 2Z_r\big)\} - Z_k\mathrm{tr}(B) + Z_r B_i^{\ k},
\end{aligned} \tag{20}$$

$$\begin{aligned}
\partial_t\theta + \partial_r(-\beta^r\theta &+ \alpha V^r) \\
= \Pi = {}& -\theta\mathrm{tr}(B) + \frac{\alpha}{2}\big[-16\pi\alpha^3 G_{00} \\
& - 2A_r\big(D_{\ kk}^r - D_k^{\ kr} - 2Z^r\big) + D_k^{\ rs}\Gamma_{rs}^k \\
& - D_{rr}^k\big(D_{ks}^{\ s} - 2Z_k\big) - K_r^k K_{kr} + \mathrm{tr}(K)^2 - 2\theta\mathrm{tr}(K)\big].
\end{aligned} \tag{21}$$

6. First-order derivatives

$$A_k = \partial_k \ln(\alpha), \quad B_i^{\ j} = \partial_i \beta^j, \quad D_{kij} = \partial_k \gamma_{ij}/2, \tag{22}$$

where $R_{ij}^{(4)}$ are the space components of the four-dimensional Ricci tensor and V_i is the Bona Masso variable defined as $V_i = D_{ir}^{\ r} - D_{ri}^{\ r} - Z_i$. Although in the original formulation of Bona-Masso equations, A_i, $B_i^{\ j}$, and D_{ijk} are considered independent variables with their own respective evolution equations, we have evolved the slicing and the metric first and then taken the derivatives. During the simulations we observed that, if they are evolved independently, then the derivative of the slicing (the metric) does not match with A_i ($B_i^{\ j}$, D_{ijk}), which leads to errors. Therefore, we will calculate them directly through α, β^i, and γ_{ij}. It must be noted that the variables (A_i, $B_i^{\ j}$, D_{ijk}) obtained through differentiation are kept in flux conservative form up to a precision determined by the numerical diffusivity η. Thus, smaller values of numerical diffusivity lead to an evolution for these quantities that is closer to the flux conservative form, and for the special case of $\eta = 0$, this form is recovered precisely. This can also be observed in

our simulations where for smaller numerical diffusivities the accuracy of our results gets better. Indeed, the model could be improved including separate equations for the fields A_i, B_i^j, and D_{ijk} to decrease as much as possible this inaccuracy, and it will be a subject of future work.

C. Gauge choices

The $3+1$ formulation does not define slice and lapse evolution uniquely, which gives us a freedom to choose the appropriate slicing and lapse depending on the system. The simplest slicing would be the geodesic slicing, $Q = 0$, and lapse, $Q_i = 0$, where the time components of the four metric stays constant throughout the simulation. However, in some situations this slicing or lapse fails to support the stability of the program, as the evolution of the metric is coupled to it. For example, geodesic slicing yields the so-called geodesic focusing problem, where the volume element goes to zero in a finite time in the presence of massive objects, thus leading to numerically unstable algorithms [7]. Other examples for slicings are the maximal slicing $\mathrm{tr}(K) = 0$, harmonic slicing $Q = \mathrm{tr}(K) - 2\theta$, and "$1 + log$" slicing $Q = \mathrm{tr}(K)/\alpha$. The maximal and $1 + log$ slicings are also known as singularity avoiding slicings [26] because they collapse the time evolution close to the singularity. The harmonic slicing corresponds to a slicing where α fulfills the wave equation $(\partial_t^2 - \partial_x^2)\alpha = 0$ [30]. In the following tests we only use the geodesic and harmonic slicings and lapses.

The tests have periodic boundary conditions. We will avoid tests that include other boundary conditions, e.g., "single Schwarzschild black holes," since they are very challenging and will need further extensions to our work.

III. LATTICE BOLTZMANN MODEL

The lattice Boltzmann Method can be used to simulate fluids or solve partial differential equations in the form of conservation laws [31]. We start with the discrete Boltzmann equation for the distribution functions, f_λ,

$$f_\lambda(x + v_\lambda \delta t, t + \delta t) - f_\lambda(x,t) = -\frac{f_\lambda(x,t) - f_\lambda^{\mathrm{eq}}(x,t)}{\tau/\delta t}, \quad (23)$$

where τ is the relaxation time, and λ denotes the discrete velocities $\{v_\lambda\}_{\lambda \in N}$. Here, we use the Bhatnagar-Gross-Krook (BGK) approximation [31], which is a small amplitude approximation for the collision term of the Boltzmann equation [right-hand side of Eq. (23)]. For an ideal gas, one can take f^{eq} as the Maxwell-Boltzmann (MB) distribution, expanded in orthogonal polynomials, and recover the Navier-Stokes equations [32]. The macroscopic fields are given by the relations

$$\rho = \sum_\lambda f^\lambda, \quad \rho u_i = \sum_\lambda v_{\lambda i} f^\lambda, \quad (24)$$

which, for the case of fluid dynamics, ρ and ρu_i are the mass and momentum densities, respectively. The lattices are described by their dimensionality (D) and amount of discrete velocity vectors (Q). An n-dimensional lattice with m velocities is denoted by DnQm. Here, we will use D2Q9 and D3Q19 for two and three dimensions, respectively. The
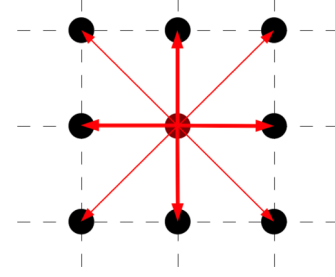
FIG. 1. D2Q9 lattice configuration vectors. The thickness of the arrows represent the weights. The dark-red point in the middle denotes the (0,0,0) vector.

D2Q9 lattice configuration is given by

$$(v_0, v_{1,2}, v_{3,4}, v_{5,6}, v_{7,8}) = \begin{pmatrix} 0 & \pm 1 & 0 & \pm 1 & \pm 1 \\ 0 & 0 & \pm 1 & \mp 1 & \pm 1 \end{pmatrix}, \quad (25)$$

where the weights are defined by $w_0 = \frac{4}{9}$, $w_{1,2,3,4} = \frac{1}{9}$, $w_{5,6,7,8} = \frac{1}{36}$, and the lattice speed of sound is given by $v_s = \frac{1}{\sqrt{3}}$ (see Fig. 1). On the other hand, the D3Q19 lattice configuration is given by

$$\begin{pmatrix} 0 & \pm 1 & 0 & 0 & \pm 1 & \pm 1 & \pm 1 & \pm 1 & 0 & 0 \\ 0 & 0 & \pm 1 & 0 & \mp 1 & \pm 1 & 0 & 0 & \pm 1 & \pm 1 \\ 0 & 0 & 0 & \pm 1 & 0 & 0 & \mp 1 & \pm 1 & \mp 1 & \pm 1 \end{pmatrix}, \quad (26)$$

with weights $w_0 = \frac{1}{3}$, $w_{1,2,3,4,5,6} = \frac{1}{18}$, $w_{\geqslant 7} = \frac{1}{36}$, and $v_s = \frac{1}{\sqrt{3}}$. Both lattices are accurate up to second order, which means that one can recover the moments of the distribution up to second order [33].

The discrete Boltzmann equation with a source term distribution $S_\lambda(x,t)$ is given by [34]

$$f_\lambda(x + v_\lambda \delta t, t + \delta t) - f_\lambda(x,t)$$
$$= -\frac{f_\lambda(x,t) - f_\lambda^{\mathrm{eq}}(x,t)}{\tau/\delta t} + \delta t\, S_\lambda(x,t). \quad (27)$$

This equation describes the evolution of the distribution functions. We calculate the equilibrium and source distributions for each component of α, β^i, γ_{ij}, θ, Z_i, and K_{ij}, such that the correct moments of the equilibrium distribution are satisfied, and consequently, the right macroscopic differential equations are recovered. Thus, one gets

$$^\alpha f_\lambda^{\mathrm{eq}} = w_\lambda \alpha, \quad (28)$$

$$^\beta f_\lambda^{i,\mathrm{eq}} = w_\lambda \beta^i, \quad (29)$$

$$^\gamma f_{ij\lambda}^{\mathrm{eq}} = w_\lambda \gamma_{ij}, \quad (30)$$

$$^z f_{i\lambda}^{\mathrm{eq}} = w_\lambda \left[Z_i \left(1 - \frac{v_\lambda^r \{ \beta^r + \alpha \delta_i^r [\mathrm{tr}(K) - \theta] - K_i^r \}}{v_s^2 v_l} \right) \right], \quad (31)$$

$$^\theta f_\lambda^{\mathrm{eq}} = w_\lambda \left\{ \theta - \frac{v_\lambda^k [\theta \beta^k - \alpha (D_{kr}^{\ r} - D_{rk}^{\ r} - Z_k)]}{v_s^2 v_l} \right\}, \quad (32)$$

$$^K f_{ij\lambda}^{\text{eq}} = w_\lambda \left[K_{ij} \left(1 - \frac{v_\lambda^k \beta^k}{v_s^2 v_l} \right) + \frac{\alpha v_\lambda^m \lambda_{ij}^m}{v_s^2 v_l} \right], \qquad (33)$$

$$^\alpha S_\lambda = w_\lambda \alpha (\beta^r A_r - \alpha Q) \left(2 - \frac{v_\lambda^2}{v_s^2} \right), \qquad (34)$$

$$^\beta S_\lambda^i = w_\lambda (\beta^r B_r^i - \alpha Q^i) \left(2 - \frac{v_\lambda^2}{v_s^2} \right), \qquad (35)$$

$$^\gamma S_{ij\lambda} = w_\lambda [2\beta^r D_{rij} - 2\alpha(K_{ij} - s_{ij})] \left(2 - \frac{v_\lambda^2}{v_s^2} \right), \qquad (36)$$

$$^Z S_{i\lambda} = w_\lambda \Omega_i \left(2 - \frac{v_\lambda^2}{v_s^2} \right), \qquad (37)$$

$$^\theta S_\lambda = w_\lambda \Pi \left(2 - \frac{v_\lambda^2}{v_s^2} \right), \qquad (38)$$

$$^K S_{ij\lambda} = w_\lambda \alpha S_{ij} \left(2 - \frac{v_\lambda^2}{v_s^2} \right), \qquad (39)$$

where the symbol $*$ at the left of the distribution and source term, $^*f$ and $^*S$, denotes the field to which f and S are associated and $v_l \equiv \delta r / \delta t$. The macroscopic variables of concern are calculated by

$$\rho^* = \sum_\lambda {}^* f_\lambda, \qquad (40)$$

where ρ^* stands for (α, β^i, γ_{ij}, θ, Z_i, K_{ij}). By performing the Chapman-Enskog expansion [34,35], one can show that the distributions and source terms recover the Z4 formulation of Einstein equations to the first order in Knudsen number [34,35]. One last remark is that we could fix the second-order moment of the equilibrium distributions to zero, but this decreases the stability of the system for two reasons: first, the equilibrium distribution can become easier negative, which violates the H-theorem leading to an unstable evolution of the system; and second, it suppresses the numerical diffusivity, which decreases the stability of the system. However, we do fix the second-order moment of the sources equal to zero, such that any spurious effect vanishes.

It is worth to mention that the lattice Boltzmann algorithm has been successfully used to study fluid dynamics as an alternative to standard solvers, such as finite volume and finite differences. Although each technique has its own advantages depending on the complexity of the problem, it has been found that by increasing the complexity of the underlying geometry, to keep the same accuracy, the lattice Boltzmann algorithm can perform more efficiently than finite-volume methods [36,37]. In fact, in terms of parallel computing, for simple geometries, finite volumes is better, while for more complex ones, there is a breaking point where lattice Boltzmann becomes faster [37]. Additionally, for time-independent problems it is expected that finite-volume methods consume less computational time; however, for time-dependent simulations lattice Boltzmann methods were found to be more efficient for the case of transport through disorder media [38]. Thus, although the advantages of lattice Boltzmann against other numerical methods are not clear for the case of numerical relativity, our model presents promising features that need to be explored in the future.

Finishing with the model description, now we will study some well-established examples in order to validate and characterize the method.

IV. TESTS AND RESULTS

In order to validate our model, we will perform the six numerical tests described in the Introduction. Four tests are on flat spacetime: Expansion of flat universe, robust stability, gauge wave, and shifted gauge wave. Finally, the last two tests correspond to curved spacetime in vacuum, namely, the linear and polarized Gowdy wave tests for weak and strong curvature, respectively. A discussion on the errors of the simulations is presented in Sec. V.

A. Expansion of flat universe

In this case, the spatial part of the energy-momentum tensor, G_{ij}, considering an ideal fluid, is given by

$$G_{00} = \rho(t) c^2, \qquad G_{ij} = P(t) \gamma_{ij}, \qquad (41)$$

where $\rho(t)$ and $P(t)$ are the density and pressure of the fluid, respectively. By solving Einstein equations for this system one obtains the Friedmann equations [39] (also knows as FLRW metric), which are

$$\frac{\dot{a}^2 + kc^2}{a^2} = \frac{9\pi G \rho + \Lambda c^2}{3}, \qquad (42)$$

$$\frac{\ddot{a}}{a} = -\frac{4\pi G}{3} \left(\rho + \frac{3P}{c^2} \right) + \frac{\Lambda c^2}{3}, \qquad (43)$$

where a is a quantity that determines the metric,

$$\gamma_{ij} = a(t)^2 \delta_{ij} = t^{\frac{2}{3}} \delta_{ij}, \qquad (44)$$

and

$$P(t) = \frac{1}{3t^2}. \qquad (45)$$

For an ideal gas with equation of state $P = \rho$ (assuming $c^2 = 8\pi G = 1$). The simulation ran using a D3Q19 lattice with $\delta t = \delta r = 0.001$, and a relaxation time $\tau/\delta t = 3$ (all values are given in numerical units). The results can be observed in Figs. 2 and 3. We have used a lattice of $4 \times 4 \times 4$ cells due to the fact that the lattice size does not matter due to isotropy and homogeneity of the problem, i.e., the expansion is the same at every position. In Figs. 2 and 3, we observe excellent agreement between the results of our simulation and the theory, showing that the universe expands following the Friedmann equations.

B. Robust stability analysis

In the robust stability analysis, the ability of the method to handle errors is tested. The errors ϵ introduced into the dynamical fields are in the range $\epsilon \in [-10^{-10}/256, 10^{-10}/256)$, and $\tau/\delta t$ is chosen to be 4.5, $\delta r = \delta t = 0.00125$. The evolution of the second fundamental form for three different resolutions and for three different $\delta r/\delta t = v_l$ ratios are given in Fig. 4. As the second fundamental form should be zero, the deviation from 0 can be interpreted as an error. We see that while for $v_l = 1$ the error increases exponentially, an increase in v_l leads
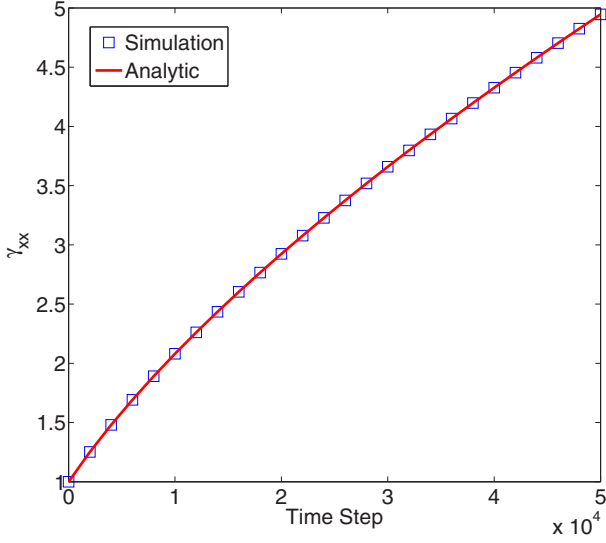
FIG. 2. Time evolution of a single component of the metric tensor for an expanding universe. The metric starts from unity and evolves according to the time dependence given in Eq. (44). The lattice size and spacing are irrelevant factors due to isotropy and flatness.

to an improvement in stability. It must be underlined that in the apples with apples tests, the equivalent of v_l is set equal to either 2 or 4.

C. Gauge wave

In this test, the metric tensor is given by

$$ds^2 = g_{\alpha\beta}dx^\alpha dx^\beta = -Hdt^2 + Hdx^2 + dy^2 + dz^2, \quad (46)$$

where $H = H(x - t) = 1 - A \sin\left(\frac{2\pi(x-t)}{d}\right)$ with d the wavelength of the gauge wave, which in our case is set to unity, and its amplitude to $A = 10^{-3}$. The extrinsic curvature can be calculated by directly taking the time derivative of the three
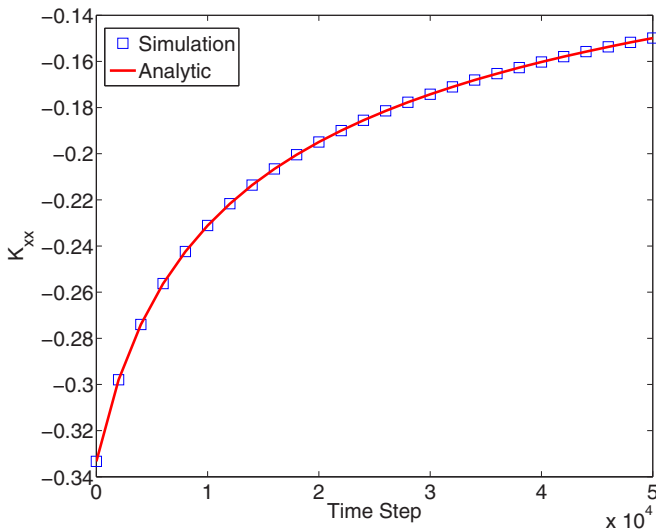
FIG. 3. Single component of the second fundamental form, K_{xx}, for an expanding universe. This fundamental form describes the time derivative of the metric via $K(t) = -\dot{a}(t)/2$.
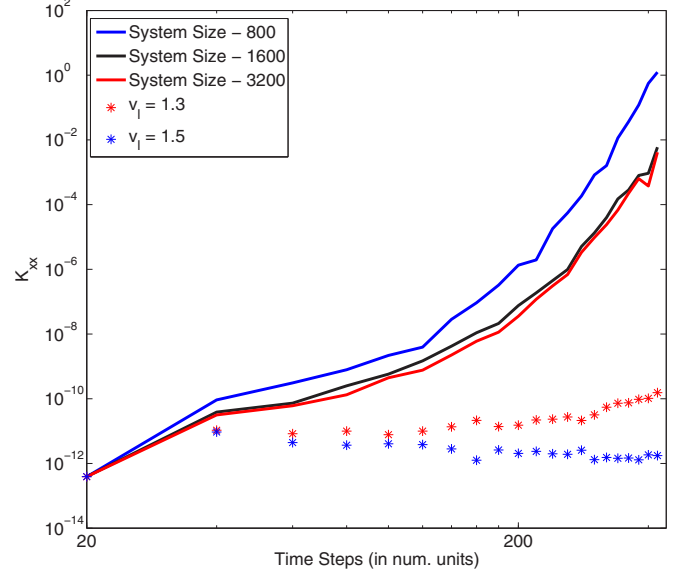
FIG. 4. We present the evolution of K_{xx}. Analytically, K_{xx} is expected to be zero, so its deviation from this value can be used as a measure of the error.

metric and dividing by -2α,

$$K_{xx} = -\frac{\pi A}{d} \frac{\cos\left(\frac{2\pi(x-t)}{d}\right)}{\sqrt{H}}, \quad K_{ij} = 0. \quad (47)$$

It can be checked by Eq. (6) that the extrinsic curvature also evolves with the time derivative of this expression. The time evolution of α is given by

$$\partial_t \alpha = -\alpha^2 Q \Rightarrow Q = \text{tr}(K) - 2\theta. \quad (48)$$

Here, we have chosen the harmonic slicing because we want $\alpha = \sqrt{H}$ to propagate also as a wave and the harmonic slicing provides a wave-like evolution to α, while keeping the evolution of the quantity H consistent with the evolution of the three metric. If the evolution of α and γ do not lead to the same equations for H, then the respective time derivatives of the extrinsic curvature do not match. The results, using $\tau/\delta t = 4.5$, are presented in Figs. 5, 6, and 7. We see again that they are in good agreement within a relative error of 1%. The simulations ran using a D2Q9 lattice configuration, where we have redefined the spatial coordinate $x \to x_r$ and keep x for the positions in the lattice, being $x_r = -400\delta r + (x - 1/2)\delta r$, and $\delta t = \delta r = 0.00125$.

D. Linear wave

In this test, we set the following metric tensor,

$$ds^2 = g_{\alpha\beta}dx^\alpha dx^\beta$$
$$= -dt^2 + dx^2 + (1+b)dy^2 + (1-b)dz^2, \quad (49)$$

where $b = A \sin\left(\frac{2\pi(x-t)}{d}\right)$ and d is the system size as above. The extrinsic curvature can be calculated directly by taking the time derivative of the three metric and dividing by -2α,
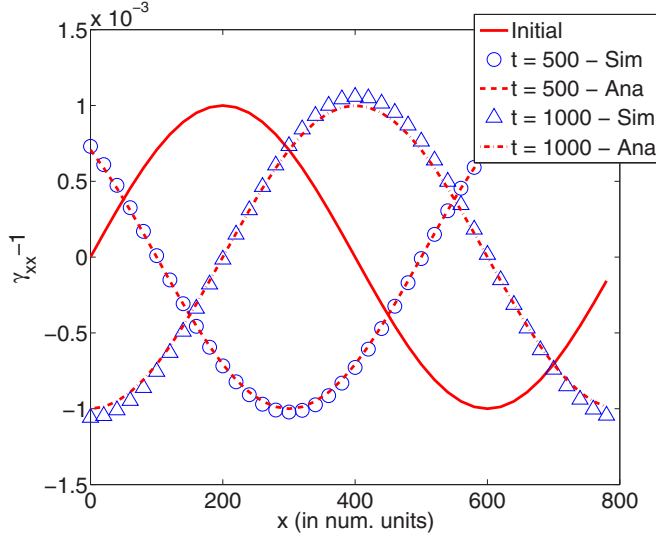
FIG. 5. The evolution of the xx component of the metric for the propagation of a gauge wave is shown at three different times. Here, t denotes the numerical time step. We see that the simulation deviates slightly from the analytical values, but the shapes are preserved and the maximum (minimum) of the waves are on the same track. "Ana" stands for analytical solution and "Sim" for simulation.

with $\alpha = 1$,

$$K_{yy} = \frac{\pi A}{d} \cos\left(\frac{2\pi(x - t)}{d}\right), \quad (50)$$

$$K_{zz} = -\frac{\pi A}{d} \cos\left(\frac{2\pi(x - t)}{d}\right). \quad (51)$$

In this case, we take geodesic slicing $Q = 0$, which would impose into the system the analytical evolution of α. As the perturbation is traceless, geodesic slicing and harmonic slicing
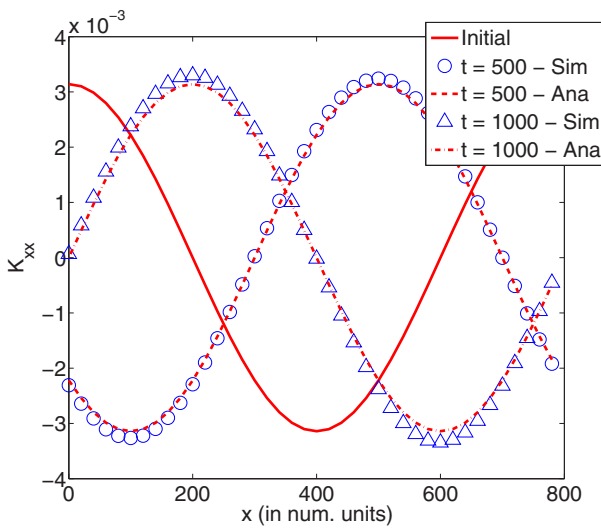
FIG. 6. The evolution of the second fundamental form for the propagation of a gauge wave is shown at three different times. We see a similar behavior to that of the metric. "Ana" stands for analytical solution and "Sim" for simulation.
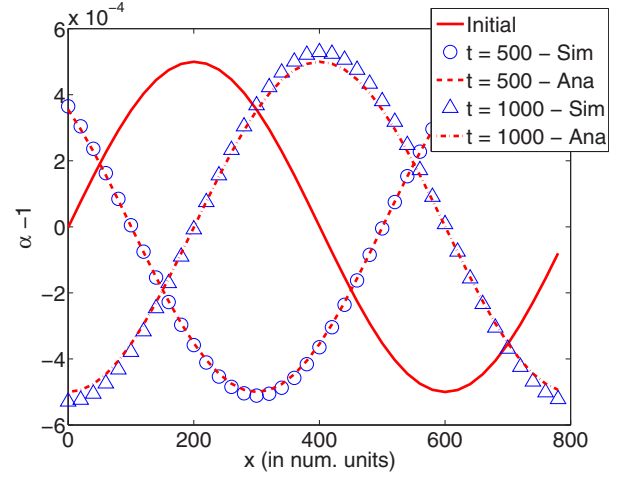
FIG. 7. The evolution of α (tt component of the metric) for the propagation of the gauge wave is shown at three different times. Here, we observe again a similar behavior to that of the metric. "Ana" stands for analytical solution and "Sim" for simulation.

are identical gauges. The amplitude is chosen as $A = 10^{-5}$. For this simulation, we use a D3Q19 lattice configuration, $\tau/\delta t = 4.5$, and the same values for x, t, and δt, δr, as before. Note that the results are very similar to those for the gauge wave, as expected (see Fig. 8).

E. Shifted gauge wave

For the shifted gauge wave, we have the following metric:

$$ds^2 = -dt^2 + dx^2 + dy^2 + dz^2 + Hk_\alpha k_\beta dx^\alpha dx^\beta, \quad (52)$$

where $k_\alpha = \partial_\alpha(t - x)$. It can be observed that this test involves the x component of the shift in addition to the variables from the earlier test for gauge wave. The solutions are given as the
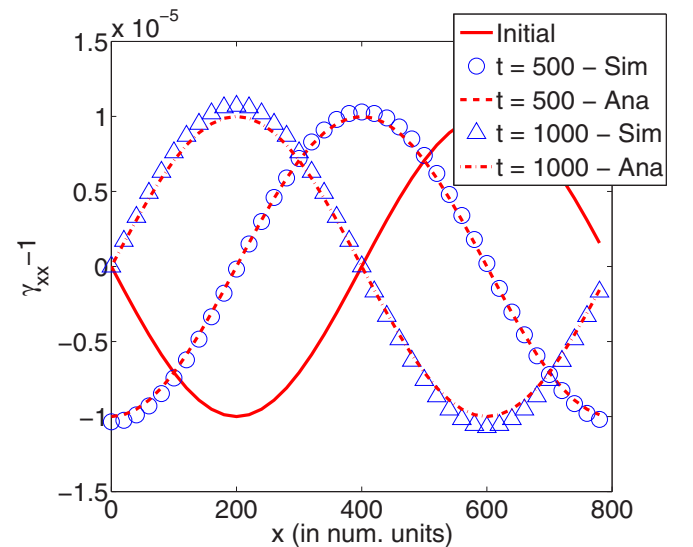
FIG. 8. Evolution of the xx component of the metric for the propagation of a linear wave at three different times t. Note that the linear wave evolves similarly to the gauge wave.
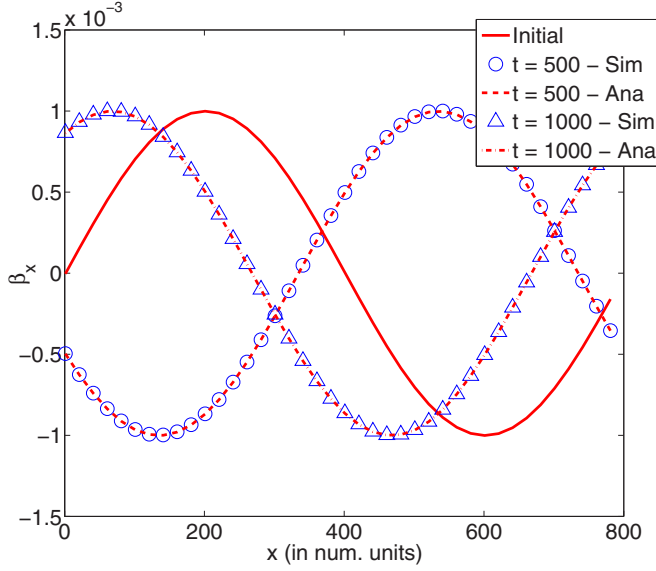
FIG. 9. The evolution of the x component of the shift for the propagation of a shifted gauge wave is shown at three different times. Here, t denotes the numerical time step. We see that the simulation almost does not deviate from the analytical values. "Ana" stands for analytical solution and "Sim" for simulation.

following:

$$\alpha = \frac{1}{\sqrt{1 + A \sin\left[\frac{2\pi(x-t)}{d}\right]}}, \tag{53}$$

$$\beta^x = \frac{-A \sin\left[\frac{2\pi(x-t)}{d}\right]}{1 + A \sin\left[\frac{2\pi(x-t)}{d}\right]}, \tag{54}$$

$$\gamma_{xx} = 1 + A \sin\left[\frac{2\pi(x-t)}{d}\right], \tag{55}$$

$$K_{xx} = \frac{-\frac{\pi A}{d} \cos\left[\frac{2\pi(x-t)}{d}\right]}{\sqrt{1 + A \sin\left[\frac{2\pi(x-t)}{d}\right]}}. \tag{56}$$

Here, we choose harmonic slicing and lapse, $Q^i = \alpha(A^i + D_r^{ir} - 2D_r^{ir} - 2Z^i)$, for the evolution of the shifted gauge wave, $v_l = 1.5$ and $\tau/\delta t = 1$. The results for β_x is given in Fig. 9. We observe better accuracy in the shifted gauge wave test than for the gauge wave test.

F. Polarized Gowdy wave

The polarized Gowdy wave is a plane polarized gravitational wave in an expanding toroidal universe. While the previous tests involve very small curvature, the Gowdy wave presents a highly curved case. It can be described by the following metric:

$$\begin{aligned} ds^2 &= g_{\alpha\beta} dx^\alpha dx^\beta \\ &= -t^{-\frac{1}{2}} e^{\frac{\lambda}{2}} (dt^2 + dz^2) + t e^P dx^2 + t e^{-P} dy^2, \end{aligned} \tag{57}$$

where λ and P are functions of z and t and periodic in z. The solutions for P and λ are given by

$$P = J_0(2\pi t) \cos(2\pi z), \tag{58}$$
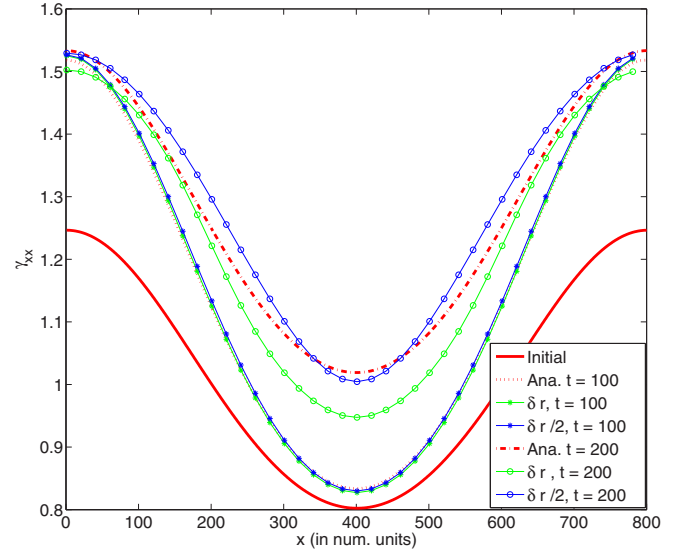
FIG. 10. The evolution of the xx component of the metric of a Gowdy wave is shown at three different times t for two different resolutions, $\delta r = 0.00125$ and $\delta r/2$. One can see that the simulation improves with higher resolution.

where J_n is the nth Bessel function and

$$\begin{aligned} \lambda &= -2\pi t J_0(2\pi t) J_1(2\pi t) \cos^2(2\pi z) + 2\pi^2 t^2 [J_0^2(2\pi t) \\ &\quad + J_1^2(2\pi t)] - \frac{1}{2} \{4\pi^2 [J_0^2(2\pi) + J_1^2(2\pi)] \\ &\quad - 2\pi J_0(2\pi) J_0(2\pi)\}. \end{aligned} \tag{59}$$

The results for the γ_{xx} are presented in Fig. 10. Here, $\tau/\delta t$ is 4.5 and $dr = dt = 0.00125$. While there is good agreement with the analytical solutions in the first 100 time steps, for later times we need to increase the resolution of the lattice to improve the results. However, a small deviation in the wavelength still remains.

V. ANALYSIS AND SIMULATION ERRORS

In this section, we analyze the errors of the performed simulations of the previous section. The tests will be analyzed in groups with the corresponding errors.

A. Errors in the validation tests

The gauge and linear waves show very similar behavior in our simulations. The evolution of the gauge wave is expected to have a finite lifetime that can be increased by improving the spatial resolution. This numerical instability is due to emerging singularities that are caused by the inaccuracy of the numerical calculations. As mentioned in Ref. [24], such system with T^3 topology must have a singularity in the future or in the past and the effect of an instability must show itself at some time during the simulation. Our simulation ran for almost 2×10^3 time steps till the relative error exceeds 10%. Compared to the well-developed methods of ADM and BSSNOK with the use of Cactus or other numerical solvers, which can handle much more time steps, our model needs improvements. This error introduced by the lattice Boltzmann model is due to the fact that singularities possess large gradients in the geometric

variables and they lead to negative equilibrium distribution functions, and consequently, to numerical instabilities. Thus, we can expect that by ensuring the H-theorem, i.e., introducing an entropic lattice Boltzmann model [40,41], one can improve drastically the model keeping its simplicity.

B. Relaxation time τ, numerical diffusivity η and $\delta r/\delta t = v_l$

Our lattice Boltzmann model has three parameters that can be adjusted, namely the relaxation time τ, the numerical diffusivity η, and the ratio of lattice distance to time steps v_l. While τ is a characteristic parameter of any lattice Boltzmann scheme and determines the diffusivity, v_l is an unusual addition to this model, which can be used to adjust the stability and accuracy of our simulations. The relaxation time τ is related to the numerical diffusivity through

$$\eta = \left(\tau - \frac{\delta t}{2}\right) v_s^2 v_l^2. \tag{60}$$

For the above tests, $\tau/\delta t$ varies between 2.5 and 5.25, and consequently, η takes values between $0.000 8\overline{3}$ and $0.002 08\overline{3}$. We see that as the relaxation time increases, the stability of the system also increases (see inset of Fig. 11), while the errors become larger (see Fig. 11). For instance, we observe that while $\tau/\delta t = 2.5$ leads to numerical instabilities quicker than $\tau/\delta t = 4.5$, it also introduces a less mean relative error into the system. Indeed, further tests show that there is an optimal value of τ for which the error introduced by the model is less while the stability is better. For instance, for the case of gravitational waves, $\tau/\delta t = 4.5$ is the optimal relaxation time.

Note that Eq. (60) states that by increasing the relaxation time, the numerical diffusivity also increases for a fixed $\delta t = \delta x$. However, one can also fix the numerical diffusivity while
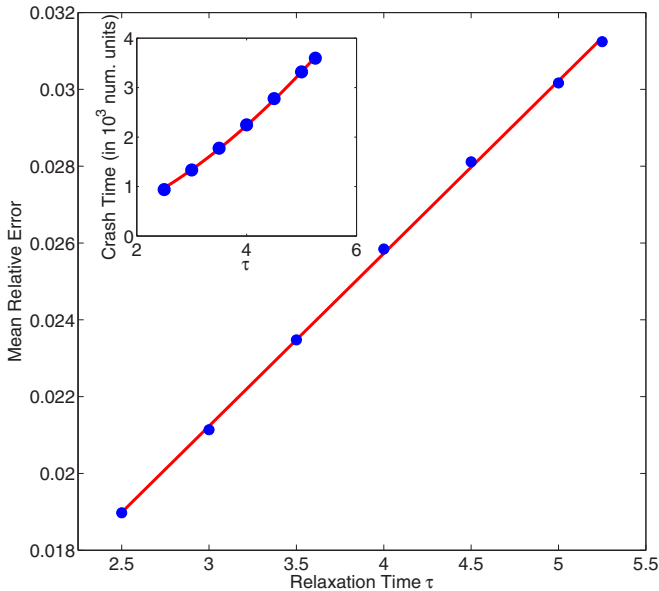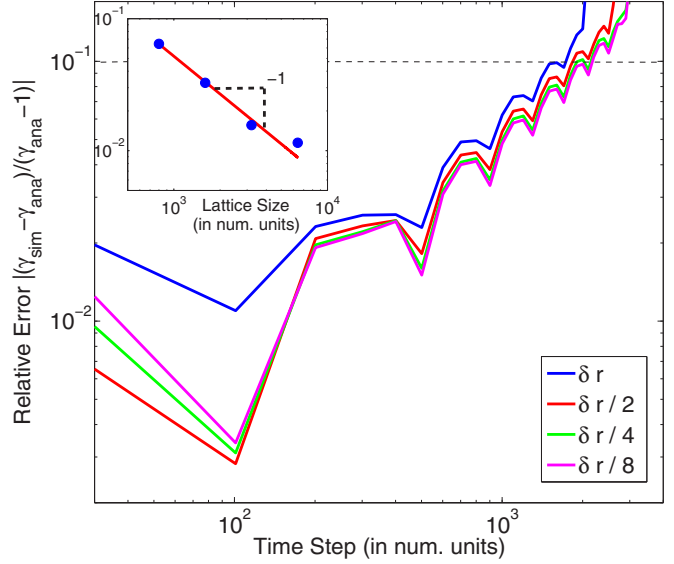
FIG. 12. Main frame: relative error of the metric for the propagation of gauge waves at different time steps for different resolutions. Here, we have kept constant the numerical diffusivity, $\eta = 0.001\overline{6}$. The errors strongly depend on the lattice spacing, and finer lattices lead to longer simulation time. Inset: we see that with finer lattices the relative error introduced at time step $400\,\delta t$ decreases as a power law showing convergency.

changing independently the relaxation time. Thus, in a second test (see Fig. 12) we study the behavior of the error when one increases the relaxation time and decreases the lattice spacing, such that the numerical diffusivity remains constant. We observe that the simulation lasts about 50% longer for the same accuracy. Therefore, we conclude that the numerical diffusivity tunes the accuracy, while the relaxation time the stability of the model. Additionally, the inset of Fig. 12 shows that the error decreases linearly with the lattice spacing (at time $t = 400\delta t$), concluding that our model converges to the analytical solution when lattice spacing is decreased.

As mentioned in the previous subsection, negative equilibrium distribution functions play an important role in terms of numerical stability. This problem usually rises when the first order moment of the distribution becomes large, and v_l is a parameter that one can freely choose to diminish its effects [see Eqs. (31)–(33)]. On the other hand, the parameter v_l also fix the integration time step when the spatial resolution is kept constant. The effect of v_l is shown in the robust stability test (Fig. 4), where one can see that by increasing v_l, the error production decreases strongly (smaller integration time step). Also in other tests, it was also observed that by increasing v_l the system becomes more stable.

FIG. 11. Mean relative error of γ_{xx} for the propagation of gravitational waves at the first 500 time steps. For higher relaxation time the accuracy gets worse. However, it can be seen, in the inset, that the lifetime of the simulation increases with increasing the relaxation time (numerical diffusivity).

VI. PARALLELIZATION OF THE CODE

Our code has been parallelized with OpenMP and tested with 1–24 cores. The results are given in the Fig. 13. The linear decrease in total computational time with respect to number of cores shows that our model is optimal for parallelization. Other more sophisticated implementations as MPI and CUDA, for GPUs, will be a subject of future works.
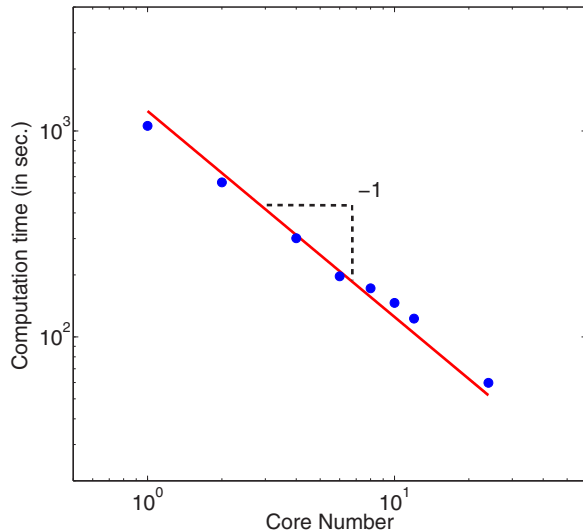
FIG. 13. Computational time as a function of the number of CPU cores. Here we observe that the computational time falls rapidly with increasing the number of CPU cores and is fitted very well by an inverse linear function.

VII. CONCLUSIONS

In summary, we have developed a lattice Boltzmann model for solving Einstein equations, using the Z4 formalism. We have validated our model with the well-established apples with apples tests. The expansion of a flat universe was recovered accurately and the wave tests showed good agreement with the analytical solutions. The role of the relaxation time and the numerical diffusivity was also studied finding that they are crucial in determining the stability and accuracy of the model. In particular, we have observed that the system gains stability (accuracy) by increasing (decreasing) the relaxation time, and therefore, an optimal value, which compromises both, can be found. More precisely, the numerical diffusivity tunes the accuracy while the relaxation time the stability of the model.

In addition to the validation tests, the inverse linear dependence of computational time with respect to the number of CPU cores was demonstrated, which is a major strength of lattice Boltzmann methods. It must be clearly underlined that with further work on this model, e.g., entropic extensions, the lattice Boltzmann method might offer new numerical advantages to numerical relativity.

[1] F. Pretorius, Phys. Rev. Lett. **95**, 121101 (2005).

[2] M. Campanelli, C. O. Lousto, P. Marronetti, and Y. Zlochower, Phys. Rev. Lett. **96**, 111101 (2006).

[3] J. G. Baker, J. Centrella, D.-I. Choi, M. Koppitz, and J. van Meter, Phys. Rev. Lett. **96**, 111102 (2006).

[4] F. Löffler, J. Faber, E. Bentivegna, T. Bode, P. Diener, R. Haas, I. Hinder, B. C. Mundim, C. D. Ott, E. Schnetter *et al.*, Classic. Quant. Gravity **29**, 115001 (2012).

[5] M. A. Scheel, H. P. Pfeiffer, L. Lindblom, L. E. Kidder, O. Rinne, and S. A. Teukolsky, Phys. Rev. D **74**, 104006 (2006).

[6] P. Anninos, K. Camarda, J. Massó, E. Seidel, W.-M. Suen, and J. Towns, Phys. Rev. D **52**, 2059 (1995).

[7] B. Brügmann, Phys. Rev. D **54**, 7361 (1996).

[8] J. Centrella, J. G. Baker, B. J. Kelly, and J. R. van Meter, Rev. Mod. Phys. **82**, 3069 (2010).

[9] L. Lindblom, M. A. Scheel, L. E. Kidder, R. Owen, and O. Rinne, Classic. Quant. Gravity **23**, S447 (2006).

[10] T. Nakamura, K. Oohara, and Y. Kojima, Prog. Theor. Phys. Suppl. **90**, 1 (1987).

[11] M. Shibata and T. Nakamura, Phys. Rev. D **52**, 5428 (1995).

[12] T. W. Baumgarte and S. L. Shapiro, Phys. Rev. D **59**, 024007 (1998).

[13] C. Bona, T. Ledvinka, C. Palenzuela, and M. Žáček, Phys. Rev. D **67**, 104005 (2003).

[14] C. Bona, J. Masso, E. Seidel, and J. Stela, Phys. Rev. D **56**, 3405 (1997).

[15] C. Bona, J. Massó, E. Seidel, and J. Stela, Phys. Rev. Lett. **75**, 600 (1995).

[16] C. Bona, C. Palenzuela-Luque, and C. Bona-Casas, *Elements of Numerical Relativity and Relativistic Hydrodynamics: From Einstein's Equations to Astrophysical Simulations*, Vol. 783 (Springer, Berlin, 2009).

[17] D. A. Wolf-Gladrow, *Lattice-gas Cellular Automata and Lattice Boltzmann Models: An Introduction*, 1725 (Springer Science & Business Media, Berlin, 2000).

[18] M. Mendoza and J. D. Munoz, Phys. Rev. E **82**, 056708 (2010).

[19] S. Succi and R. Benzi, Physica D: Nonlin. Phenom. **69**, 327 (1993).

[20] M. Mendoza, B. M. Boghosian, H. J. Herrmann, and S. Succi, Phys. Rev. Lett. **105**, 014502 (2010).

[21] M. Mendoza, S. Succi, and H. J. Herrmann, Phys. Rev. Lett. **113**, 096402 (2014).

[22] M. Mendoza, S. Succi, and H. J. Herrmann, Sci. Rep. **3**, 3106 (2013).

[23] M. Mendoza, A. Kaydul, L. de Arcangelis, J. S. Andrade, Jr., and H. J. Herrmann, Nature commun. **5**, 5035 (2014).

[24] M. Alcubierre, G. Allen, C. Bona, D. Fiske, T. Goodale, F. S. Guzmán, I. Hawke, S. H. Hawley, S. Husa, M. Koppitz *et al.*, Classic. Quant. Gravity **21**, 589 (2004).

[25] M. C. Babiuc, S. Husa, D. Alic, I. Hinder, C. Lechner, E. Schnetter, B. Szilagyi, Y. Zlochower, N. Dorband, D. Pollney *et al.*, Classic. Quant. Gravity **25**, 125012 (2008).

[26] M. Alcubierre, *Introduction to 3+ 1 Numerical Relativity* (Oxford University Press, Oxford, 2008).

[27] R. Arnowitt, S. Deser, and C. W. Misner, Gen. Relativ. Gravit. **40**, 1997 (2008).

[28] C. Bona, L. Lehner, and C. Palenzuela-Luque, Phys. Rev. D **72**, 104009 (2005).

[29] D. Alic, C. Bona-Casas, C. Bona, L. Rezzolla, and C. Palenzuela, Phys. Rev. D **85**, 064040 (2012).

[30] A. Geyer and H. Herold, Phys. Rev. D **52**, 6182 (1995).

[31] C. Peng, Masters Thesis in Math, Department of Mathematics, Ecole Polytechnique Federale de Lausanne, 2011.

[32] X. He and L.-S. Luo, Phys. Rev. E **56**, 6811 (1997).

[33] S. S. Chikatamarla and I. V. Karlin, Phys. Rev. E **79**, 046701 (2009).

[34] J. M. Buick and C. A. Greated, Phys. Rev. E **61**, 5307 (2000).

[35] Z. Guo, C. Zheng, and B. Shi, Phys. Rev. E **65**, 046308 (2002).

[36] Y. Y. Al-Jahmany, G. Brenner, and P. O. Brunn, Int. J. Numer. Methods Fluids **46**, 903 (2004).

[37] J. Bernsdorf, F. Durst, and M. Schäfer, Int. J. Numer. Methods Fluids **29**, 251 (1999).

[38] S. Geller, M. Krafczyk, J. Tölke, S. Turek, and J. Hron, *Proceedings of the First International Conference for Mesoscopic Methods in Engineering and Science* [Comput. Fluids **35**, 888 (2006)].

[39] A. Friedman, Gen. Relativ. Gravit. **31**, 1991 (1999).

[40] I. Karlin, A. Ferrante, and H. Öttinger, Europhys. Lett. **47**, 182 (1999).

[41] B. M. Boghosian, P. J. Love, P. V. Coveney, I. V. Karlin, S. Succi, and J. Yepez, Phys. Rev. E **68**, 025103 (2003).